CrossMark

Experimental and Numerical Study of the Influence of Gas Pressure on Gas Permeability in Pressure Relief Gas Drainage

Cun Zhang[1,2,3] · Lei Zhang[4] · Shihao Tu[4] · Dingyi Hao[4] · Teng Teng[1,2,3]

Abstract

Changes in gas pressure or external stress cause changes in permeability; furthermore, the severity of stress disturbance in these situations can easily produce plastic yielding in the coal seam. Variations in coal seam permeability are also different between the elastic and plastic zones during the process of gas drainage. Therefore, it is necessary to consider gas pressure and external stress during pressure relief gas drainage in order to provide guidance for drilling in terms of location, timing, and pressure. An experimental study explored the relationship between external stress, gas pressure, and permeability in elastic and plastic fracture coal samples. This paper then conducts a numerical simulation of gas drainage according to the model, using the FISH programming language embedded in the FLAC3D numerical simulation software. The experimental results demonstrate that permeability in elastic coal samples first decreased and then increased with increasing gas pressure; in contrast, permeability in fractured coal samples decreased with increasing gas pressure and did not appear to increase at all within the tested gas pressure range. Decreases in permeability accompanied increases in gas pressure under constant effective stress; this indicates that decreases in effective stress lead to increases in permeability when the gas pressure exceeds the critical gas pressure under constant external stress. In contrast, when the gas pressure is less than the critical value, the Klinkenberg effect and matrix adsorption expansion play a major role in permeability changes. The influence of the Klinkenberg effect and adsorption on permeability decreases as gas pressure increases under the same effective stress or external stress conditions. Permeability and its sensitivity to gas pressure decrease with increasing effective stress or external stress. Meanwhile, the simulation demonstrates that permeability in the plastic zone increases in a nonlinear fashion as gas pressure decreases. These permeability increases can be divided into four stages: a rapid increase, gradual smoothing, a second slow increase, and ultimate stability.

Keywords Permeability · Gas pressure · Effective stress · Pressure relief gas drainage · Numerical simulation

---

Extended author information available on the last page of the article

1 Introduction

The permeability of a coal seam directly affects its gas drainage efficiency, such that improving permeability has become a major focus of research in the field. In fact, the relationship between stress and permeability is the main research topic in laboratory experiments and it provides the most extensive theoretical basis for field applications. In studying the relationship between stress and permeability, scholars have used theoretical analysis and laboratory experiments to establish various theoretical models, including the Palmer and Mansoori (P&M) model, the Shi and Durucan (S&D) model, the Cui and Bustin (C&B) model, and the improved P&M model (Shi and Durucan 2013; Cui and Bustin 2005; Palmer 2009). In these models, stress refers to effective stress in general; based on Biot's theory, effective stress is defined as follows (Jaeger et al. 2007):

$$\sigma = \sigma_t - \alpha P \tag{1}$$

where σ_t is the total stress, P is the fluid pressure, and α is the Biot's coefficient. Here, the compressive stress is considered to be positive. Previous studies (Shi et al. 2004) established that the value of Biot's coefficient can always be considered to be 1 (Liu and Rutqvist 2010). Regarding effective stress as a variable, the characteristics of variations in the gas permeability of loaded methane-containing coal have been studied under different confining pressures and pore pressures using various experimental apparatus (Lv 2012; Yin et al. 2015; Li et al. 2014). However, the above models are applicable for the cases of oil and gas extraction with small stress disturbance or for the elastic coal samples. In the pressure relief coal mining, the overburden strata above the mining seam are conventionally subdivided (from the bottom to the top) into "three vertical zones" and they are caved zone, fractured zone and bending zone from the bottom to the top, as shown in Fig. 1 (Palchik 2003, 2010; Cheng et al. 2017). The coal and rock masses in the fractured zone are usually subjected to shear or tensile damages, their fracture is more developed and permeability is greatly increased, promoting gas migration. Thus, the fractured and elastic coal samples are the main research object of this study. The above classic models for the elastic coal samples linking stresses and permeability can not be well used in the studies of fractured coals in this paper.

Although gas pressure has been taken into account with regard to the influence of effective stress on permeability, experimental results indicate that under equivalent effective stress, changes in gas pressure lead to corresponding permeability changes. The main factors that affect the permeability during gas pressure changes include the adsorption of coal, changes in effective stress, Klinkenberg effect under low gas pressure conditions and the Non-Darcy flow behavior under high gas pressure difference (Yuan et al. 2014; Moghaddam and Jamiolahmady 2016; Li et al. 2014; George and Barakat 2001; Chen et al. 2015). In the case of constant external stress, coal's effective stress decreases with increases in gas pressure and permeability. However, an increase in gas pressure also increases the amount of gas adsorbed by coal, causing the coal matrix to expand and the pore space to decrease.

According to this process, gas adsorption appears to affect coal and rock permeability. In turn, volumetric shrinkage associated with gas desorption from the coal matrix has a significant influence on the stress field and changes the effective stress (George and Barakat 2001; Yi et al. 2009). Liu and Rutqvist (2010) proposed a formula for effective stress calculation that takes internal swelling stress into account:

$$\sigma = \sigma_t - \alpha P + \sigma_I \tag{2}$$

Note that σ_I is positive for matrix swelling and negative for matrix shrinkage. Using this formula, researchers conducted a series of permeability and strain measurements after
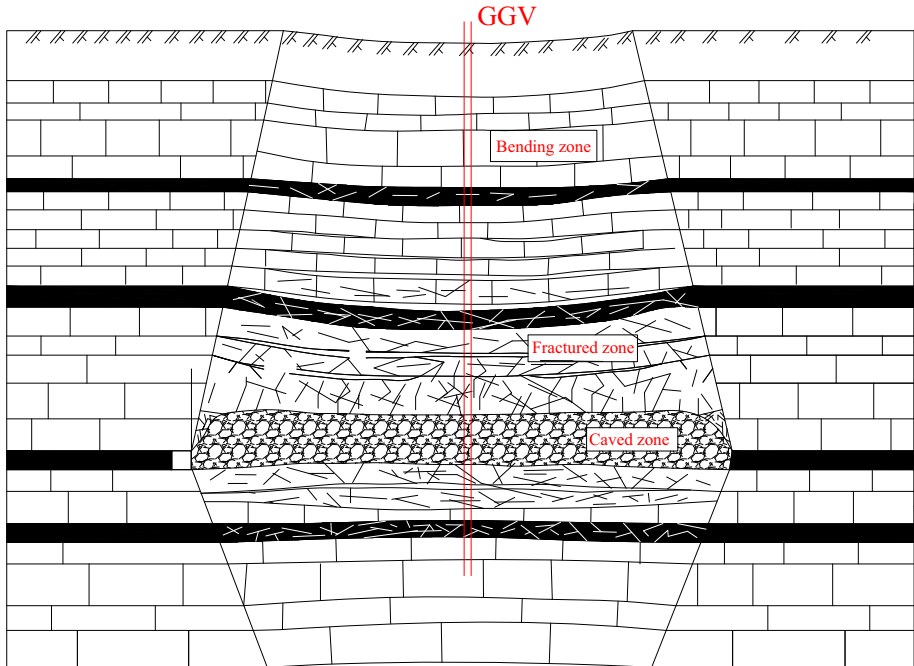
Fig. 1 Three vertical zones after coal mining

different gas adsorption equilibration at various pore and confining pressures (Pan et al. 2010; Espinoza et al. 2014).

The Klinkenberg effect generally occurs when gas pressure is relatively minor, and it is more obvious under conditions of low gas pressure and low external stress (Wang et al. 2016). Zhou et al. (2016) proposed that the Klinkenberg coefficient, which is closely related to the width of the gas flow path, cannot be treated as a constant. The coal cleat width changes because of compressibility and sorption-induced strain features.

However, many of the findings discussed above are based on coalbed methane (CBM) extraction, in which the external stress disturbance is relatively small, and dynamic changes in permeability are mainly caused by decreasing gas pressure during the process of extraction (Tao et al. 2012; Coletta and Sicco 2012; Salmachi and Yarmohammadtooski 2015). In contrast, the external stress disturbance is more intense during the process of gas drainage in coal seam group pressure relief mining. Furthermore, the severe disturbance created by stress can easily produce plastic yielding in the coal seam and formed the fractured zone (Fig. 1). Due to the fracture structure of coal seam has a great influence on permeability (Yarmohammadtooski et al. 2017); variations in coal seam permeability during the process of gas drainage are also different between the elastic and plastic fracture zones. Because changes in external stress and gas pressure both cause changes in coal seam permeability, it is necessary to consider these two factors during gas drainage to provide guidance for drilling parameters such as location, timing, and pressure.

This paper describes a laboratory investigation into elastic and shear fractured coal samples in the Huainan coal mine. An experimental study was conducted to explore the stress–gas pressure–permeability relationship of elastic and shear failure coal samples. Based on the experimental findings, this paper proposes a stress–gas pressure–permeability model for the fractured zone and bedding zone during pressure relief gas drainage. Finally, a numerical
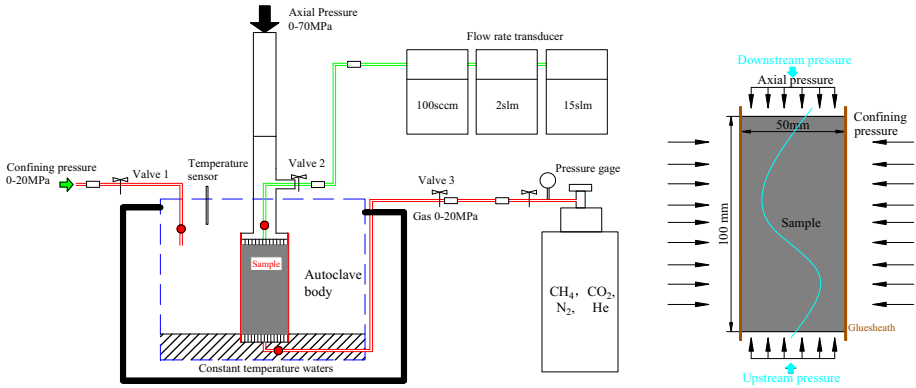
Fig. 2 Schematic diagram of the axial permeability test

simulation of gas drainage is carried out according to the stress–gas pressure–permeability model using the FISH programming language embedded in the FLAC3D numerical simulation software.

2 Experimental Schemes

2.1 Experimental Methods and Equipment

This paper uses effective stress σ_1, which comprises axial stress σ_2, confining stress σ_3, and gas pressure P. When the axial stress is equal to the confining stress, the formula for calculating effective stress is as follows:

$$\sigma_1 = (\sigma_2 + 2\sigma_3)/3 - P \tag{3}$$

This paper also adopts the steady-state method for permeability tests, and the experimental equipment is shown in Fig. 2. Equation (4) is the formula for calculating gas permeability in the steady-state permeability test:

$$K = \frac{2P_0 Q_0 \mu L}{A(P_1^2 - P_2^2)} \tag{4}$$

where K is gas permeability, md; A is the cross-sectional area of coal samples, cm^2; L is the length of the coal sample, cm; P_0, P_1, and P_2 are atmospheric pressure, upstream pressure and downstream pressure, respectively, MPa; μ is the viscosity of the gas, MPa s; and Q_0 is the flow rates under atmospheric pressure, cm^3/s.

2.2 Coal Sample Preparation

The test samples were drawn from the 13-1 coal seam in the Huainan coalfield. The average cover depth and thickness of the coal seam are 870 and 4.03 m, respectively. The gas content and the highest gas pressure in the 13-1 coal seam are 8.78 m^3/t and 3.7 MPa, respectively. The original permeability of the 13-1 coal seam is 0.002 md measured by the underground in situ permeability test method. This coal seam belongs to the outburst coal seam. Table 1 shows the test results for proximate analysis, adsorption, and constants a and b, while Table 2

Table 1 Coal proximate analysis and adsorption of a and b constant determination results

Mad (%)	Aad (%)	Vad (%)	St.ad (%)	TRD (g/cm^3)	A	b
1.70	18.28	29.75	0.10	1.67	8.521	2.133

Table 2 Physical and mechanical parameters of the coal samples

Elastic modulus E_m	Poisson's ratio ν_m	Cohesion c_m	Tensile strength t_m	Friction angle φ_m	Compressive strength σ_m
1.59 GPa	0.15	3.14 MPa	1.09 MPa	37.13°	15.98

(a)

(b)

Fig. 3 Coal samples in the permeability test. **a** Elastic coal samples, **b** plastic fracture coal samples

shows the physical and mechanical parameters of the coal samples. In Table 1, Mad, Aad, Vad, St.ad and TRD are the abbreviation of moisture air-dried basis, ash air-dried basis, volatiles air-dried basis, sulphur total air-dried basis and true relative density. The reflectance of the vitrinite group of the coal sample is mostly between 0.70 and 0.95%, which belongs to the stage of low metamorphic bituminous coal to medium metamorphic bituminous coal. This experiment used raw coal samples with sizes of ϕ50 mm × 50 mm and ϕ50 mm × 100 mm, as shown in Fig. 3a. These are direct drilling from the coal seam in bending zone (Fig. 1), fractures in these coal samples are not developed and they are in elastic stage. Shear tests were carried out on the elastic coal samples; additionally, coal samples with shear failure, where the shear fracture plane was perpendicular to the coal sample ends, were selected for further experimental study of the plastic fracture coal sample, as shown in Fig. 3b.
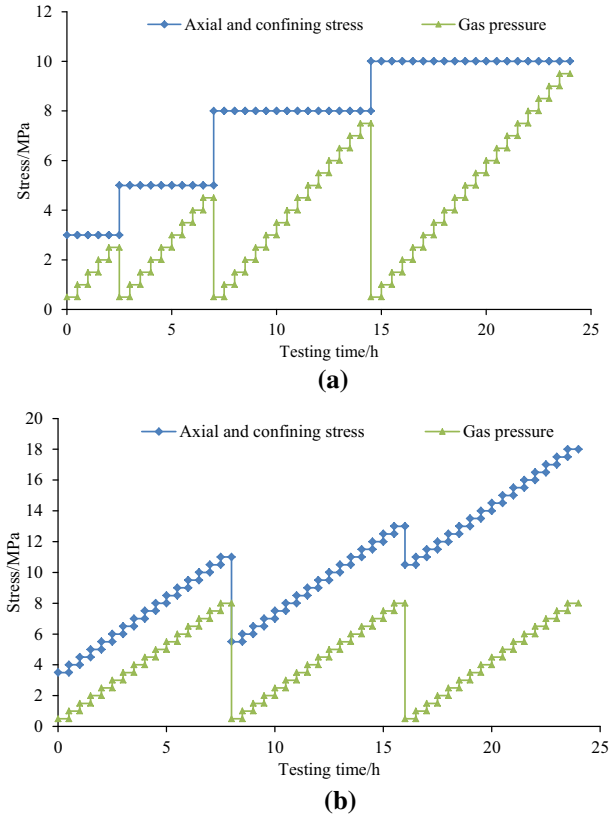
Fig. 4 Stress path of the seepage experiment. **a** Constant external stress, **b** constant effective stress

2.3 Experiment Stress Path

To study the evolution of coal's permeability during pressure relief gas extraction, the experimental stress path shown in Fig. 4 was combined with the actual stress distribution of the coal seam. Figure 4 shows two kinds of stress paths, for constant external stress and constant effective stress. The external stress is the stress applied in the coal samples including the axial and confining stress. Constant external stress means that the axial and confining stress are equal and remain constant when the gas pressure rises. Thus, the external stress in this paper is equal to the axial stress or confining stress. Constant effective stress means that the axial and confining stress change according to Eq. (3) in order to keep the effective stress unchanged. Before the permeability test, the gas pressure was applied to the predetermined value (Fig. 4), and the sample was adsorbed to the adsorption equilibrium under the each external stress condition in Fig. 4. Because of the high permeability of plastic fracture coal samples, it is very easy for the flow rate of high-pressure gas to exceed the flow meter range; therefore, the maximum gas pressure depends on the meter range. The constant external stresses were 3, 5, 8, and 10 MPa. The gas pressure increased from 0.5 MPa to the final pressure, which was 0.5 MPa less than the external stress, at intervals of 0.5 MPa. The constant effective stresses were 3, 5, and 10 MPa, while the gas pressure increased from 0.5 to 5 MPa.

2.4 The Effect of the Gas Pressure Difference on Permeability

It can be seen from the above stress path that the variation of gas pressure difference is large. The change of gas pressure difference will change the flow state of gas and affect the calculation of permeability. The two main factors that affect the permeability include the Klinkenberg effect in the low gas pressure range and the non-Darcy flow in the high gas pressure range.

(1) Klinkenberg effect

In1941, Klinkenberg proposed that the slippage effect would occur when natural gas flow through porous media in the absence of connate water (Klinkenberg 1941). The relationship between the gas permeability and the absolute permeability was also given.

$$K_D = K_a\left(1 + \frac{4c\lambda}{R}\right) \tag{5}$$

where K_D is the Darcy permeability, K_a is the absolute permeability; c is the proportional factor; λ is the mean free path of gas molecules and R is the average radius of the pore. Since then, many scholars have found that the mean free path of gas molecules is inverse to the average pore pressure through experiments. Thus, Eq. (1) can be also expressed as:

$$K_D = K_a\left(1 + \frac{b_k}{P_m}\right) \tag{6}$$

where b_k is the slippage factor and it reflects the strength of the gas slipping effect, the greater the slippage factor, the greater the gas slippage effect. When the slip factor is zero, the gas flow is Darcy flow. In recent years, some scholars have found that although the Klinkenberg formula explains the gas of porous media with large permeability, there is a large deviation in the gas slippage effect of low permeable porous media (Fathi et al. 2012; Wang et al. 2014). This is because the Klinkenberg formula is based on the assumption that the velocity gradient in the capillary is constant, but the velocity gradient in the actual capillary is not a constant. A two quadratic function is proposed by Moghadam and Chalaturnyk (2014) to explain the slippage effect of low permeability porous media based on the assumption that the velocity gradient in the capillary is reduced with the increase of the distance from the tube wall. In Eq. (7), a_k is the secondary slippage factor.

$$K_D = K_a\left(1 + \frac{b_k}{P_m} - \frac{a_k}{P_m^2}\right) \tag{7}$$

(2) Non-Darcy flow behavior

At low flow rates, the pressure drop is linearly proportional to the flow rate when the flow through porous media is described by Darcy equation:

$$-\frac{dp}{dx} = \frac{\mu v}{K_D} \tag{8}$$

where x represents the distance, p is the pressure, v is the velocity, and μ is the dynamic fluid viscosity. As the flow rates increase, the Darcy's law no longer holds; the relationship between pressure gradient and velocity becomes nonlinear due to the inertial effects. The phenomenon is known as the non-Darcy flow behavior, which is described by Forchheimer equation (Muljadi et al. 2016):

$$-\frac{dp}{dx} = \frac{\mu v}{K_F} + \rho\beta v^2 \tag{9}$$

Table 3 Basic parameters of coal samples

No.	Sample ID	Length (mm)	Diameter (mm)	Coal sample type
1	P1	99.53	50.15	Elastic coal samples
2	P2	98.93	49.83	
3	P3	99.07	50.42	
5	S1	51.25	51.18	Plastic fracture coal samples
6	S2	51.13	52.39	
7	S3	50.79	52.04	

where ρ is the fluid density, K_F is the Forchheimer permeability which is close but not equal to K_D, and β is the non-Darcy coefficient of porous medium. According to Eqs. (8) and (9), the relationship between Darcy permeability and Forchheimer permeability was as follows:

$$\frac{\mu\nu}{K_D} = \frac{\mu\nu}{K_F} + \rho\beta\nu^2 \tag{10}$$

It can be seen from Eqs. (7) and (10), whether it is in a low pressure range or a high-pressure range, that the Darcy permeability is not equal to the absolute permeability. With the gas pressure increase, the Klinkenberg effect gradually decreased according to Eq. (7). It will cause the Darcy permeability gradually decreases. While Non-Darcy flow behavior gradually enhanced with the gas pressure increase due to the gas velocity increase according to Eq. (10). Thus, with the gas pressure increase, the Darcy permeability first decreases and then increases.

In this paper, Darcy permeability is used to analyze the relations of external stress, gas pressure and permeability. The Darcy permeability is just a value for the permeability model; it is calculated by the Darcy equation. Based on this Darcy permeability, the real flow can be calculated based on Darcy equation. Moreover, the flow equations in FLAC3D are also the Darcy equation; it means that the permeability must be the Darcy permeability for the numerical simulation. According to the analysis above, the Darcy permeability first decrease and then increase with the gas pressure increase. And it can be seen from the Eqs. (7) and (10) that the Darcy permeability and gas pressure are related to quadratic function. Thus, the empirical equations of quadratic function were used in this paper, and previous studies show that the quadratic function can well match the experimental data (Yuan et al. 2014; Cao et al. 2010).

3 Experimental Results and Analysis

3.1 Permeability Changes of Elastic Coal Samples with Different Gas Pressures and External Stresses

This study employed three coal samples for the seepage experiment, with the specific parameters of the coal samples shown in Table 3. The test results are shown in Fig. 5.

The data in Fig. 5a indicate that permeability first decreased and then increased with increasing gas pressure, consistent with the quadratic function curve. The fitting formula ($y = aP^2 + bP + c$) and the critical
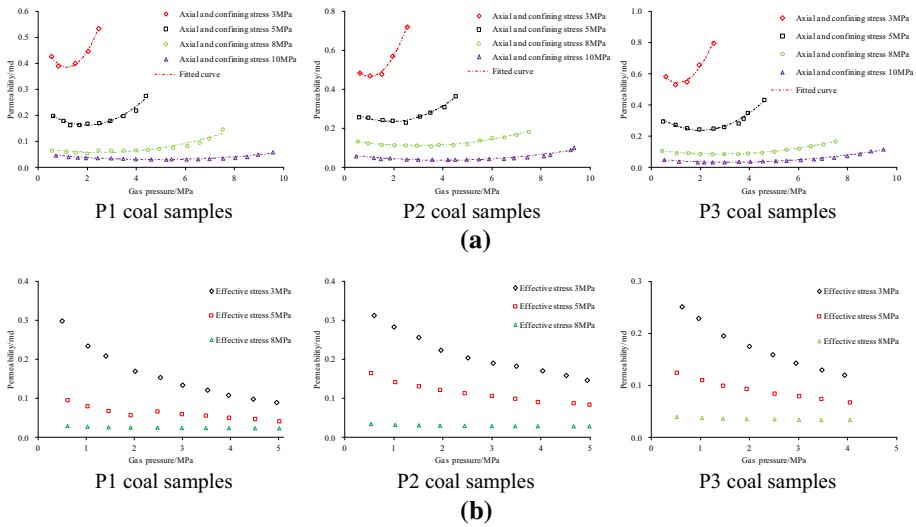
Fig. 5 Experimental results of the elastic coal samples under different stress conditions. **a** Constant external stress, **b** constant effective stress

Table 4 Fitting results of the experimental data under constant external stress

Sample ID	External stress (MPa)	Fitting formulas of permeability (md)	R^2	Critical gas pressure (MPa)/permeability (md)
P1	3	$k = 0.0903P^2 - 0.211P + 0.509$	0.9907	1.168/0.386
	5	$k = 0.018P^2 - 0.0715P + 0.2335$	0.9571	1.986/0.162
	8	$k = 0.0029P^2 - 0.0159P + 0.0762$	0.9084	2.741/0.054
	10	$k = 0.0014P^2 - 0.0096P + 0.053$	0.8975	3.429/0.033
P2	3	$k = 0.1111P^2 - 0.2249P + 0.5798$	0.9929	1.012/0.466
	5	$k = 0.0179P^2 - 0.0773P + 0.2986$	0.9705	2.159/0.215
	8	$k = 0.0035P^2 - 0.0206P + 0.1419$	0.9079	2.943/0.112
	10	$k = 0.0018P^2 - 0.0127P + 0.0665$	0.9122	3.528/0.044
P3	3	$k = 0.1232P^2 - 0.2637P + 0.6843$	0.9795	1.070/0.543
	5	$k = 0.0282P^2 - 0.1136P + 0.3525$	0.9684	2.014/0.238
	8	$k = 0.0028P^2 - 0.0172P + 0.0951$	0.9267	3.071/0.069
	10	$k = 0.0019P^2 - 0.0139P + 0.0538$	0.9782	3.656/0.028

gas pressure can be obtained by fitting of the experimental data, as shown in Table 4. Additionally, under conditions of constant external stress, permeability and its stress sensitivity decreased with increases in external stress. When the gas pressure is less than its critical value, the Klinkenberg effect and matrix adsorption expansion play a major role in changing permeability. The decrease in effective stress, which leads to increased pore space, plays the leading role when the gas pressure exceeds its critical value.
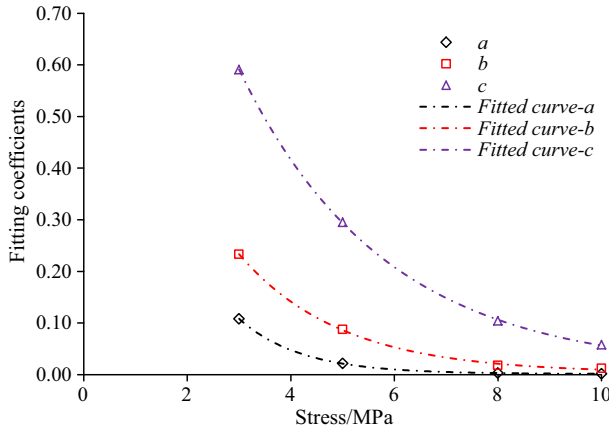
Fig. 6 Fitting curves of the fitting parameters (a, b, c)

To study the influence of the Klinkenberg effect and matrix adsorption expansion on permeability in more detail, this study explored gas pressure changes under constant effective stress (Fig. 5b). The data in Fig. 5b show that permeability decreased with increasing gas pressure and did not appear to increase under constant effective stress. The data also indicate that decreasing effective stress caused increased permeability under conditions of constant external stress. The influence of the Klinkenberg effect and adsorption on permeability appears to decrease as gas pressure increases under the same effective stress conditions; furthermore, permeability and its sensitivity to gas pressure appear to decrease with increases in effective stress.

The data in Table 4 show that the quadratic function has a good fitting effect. They also show that the chosen fitting formula can adequately approximate permeability changes with gas pressure under constant stress. The fitting formula coefficients (a, b, c) are affected by external stress in a negative exponential relationship, as shown in Fig. 6.

The fitting coefficients (a, b, c) in Fig. 6 are the average value of the three coal samples, and the correlation coefficient of the fitting coefficients is more than 0.99. Therefore, the permeability model for different external stress σ_h and gas pressure can be expressed as Eq. (11):

$$k_p = \left(0.0014 + 1.3197e^{-0.8382\sigma_h}\right) P^2$$
$$- \left(0.0032 + 1.0625e^{-0.5098\sigma_h}\right) P + 1.7002e^{-0.3570\sigma_h} + 0.0086 \qquad (11)$$

3.2 Permeability Changes of Plastic Fracture Coal Samples with Different Gas Pressure and External Stress

Three plastic fracture coal samples were subjected to seepage experiments, with the specific parameters of the coal samples shown in Table 3. The test results are shown in Fig. 7.

Unlike in the elastic coal samples, the permeability of the fractured coal samples decreased with increases in gas pressure and did not appear to increase within the range of the gas pressure tests. It is possible that the gas pressure did not increase to the critical level because
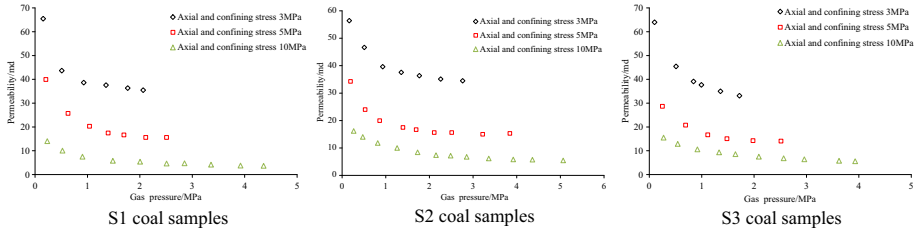
Fig. 7 Experimental results of the plastic fracture coal samples under constant external stress

of the limited flow meter range; however, the maximum gas pressure of the plastic fracture coal sample exceeds the critical gas pressure of the elastic coal sample in the same external stress state. In addition, permeability sensitivity to gas pressure varies widely in different gas pressure stages. For example, permeability significantly decreases with increasing gas pressure when gas pressure remains below 1 MPa; thereafter, permeability decreases slowly as gas pressure continues to increase. This phenomenon may be caused by the Klinkenberg effect, the velocity sensitivity effect, and the matrix adsorption expansion. The velocity sensitivity effect exists due to the high permeability of the fractured coal sample, and the increased gas flow rate in the initial stage of increasing gas pressure attenuates permeability (Wang and Le 2009). According to the elastic coal sample fitting method, Eq. (3) outlines the gas permeability model under different gas pressures and external stresses. Because permeability decreased throughout the experimental process, this paper uses the exponential function for fitting.

$$k_{\mathrm{S}} = \left(11.7736 + 103.3286\mathrm{e}^{-0.4323\sigma}\mathrm{h}\right)\mathrm{e}^{-\left(0.93+5.0421\mathrm{e}^{-0..3588\sigma_h}\right)P}$$
$$+ 147.7816\mathrm{e}^{-0.5284\sigma}\mathrm{h} + 4.2106 \tag{12}$$

where k_{s} is the permeability of the plastic fracture coal sample. During the process of pressure relief gas drainage, gas pressure in the coal seam continues to decline with gas extraction, and permeability also varies with different zones (bedding zone and fracture zone) and different stress states. Therefore, it is necessary to consider these three factors (gas pressure, stress state, and fracture development) when calculating permeability during pressure relief gas drainage. This next section of this paper carries out numerical simulations of gas drainage based on the permeability model fitted with the experimental data described above.

4 Numerical Simulation of Gas Drainage in Coal Seam

4.1 Establishment of Numerical Model

During the actual process of pressure relief gas drainage, the stress environment of a coal seam changes constantly. For the sake of efficiency, this model carries out the seepage calculation after the mechanics calculation balances. Permeability is then continuously renewed according to the state of the coal seam and gas pressure, as shown in Fig. 8.

The size of the small gas drainage model was $1 \times 1 \times 0.1$ m. In the numerical modeling, bedding zone in Fig. 1 after pressure relief mining was simulated; the horizontal and vertical stresses were reduced to 7.2 and 6 MPa, respectively, as shown in Fig. 9. The bottom of the model and the surrounding boundary are fixed. The cohesive softening model was used in

Fig. 8 The calculation program of seepage calculation for pressure relief gas drainage
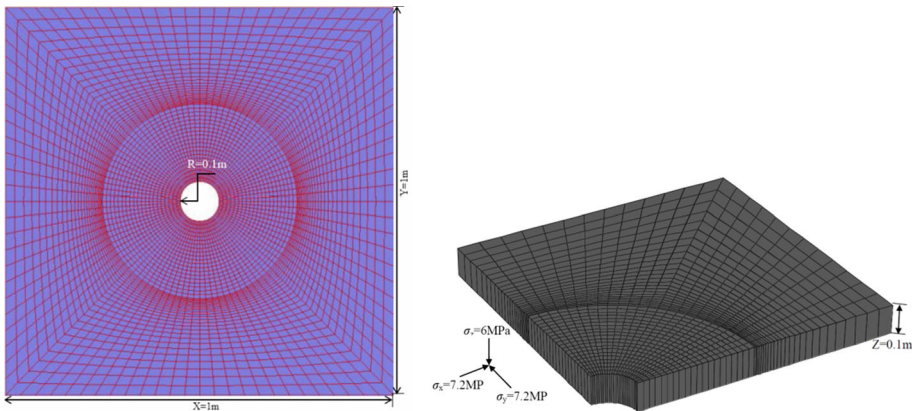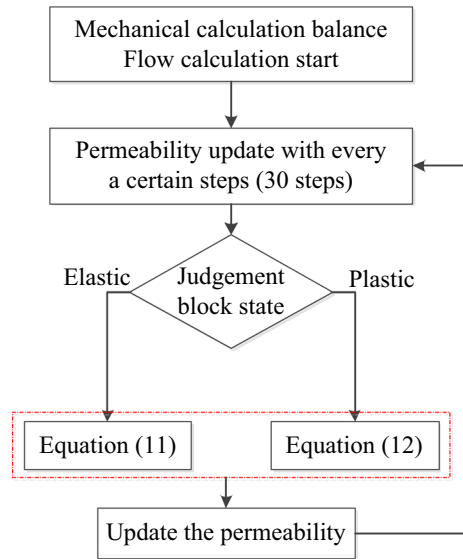

Fig. 9 Numerical model of gas extraction

this paper according to the following Eqs. (13) and (14) using FISH language in the process of mechanical calculation. The mechanical parameters of coal seam are listed in Table 2. The diameter of the borehole was 200 mm, much smaller than the size of the model; therefore, the borehole has little influence on the permeability distribution and evolution of the whole model and only affects the surrounding rock within a certain range.

Previous studies proposed the three-zone model by means of theoretical analysis, numerical simulation, and field measurement (Yao et al. 2010; Huang et al. 2013). From the inside to the outside of the drilling area, the three zones are the broken zone, plastic zone, and elastic zone, as shown in Fig. 10. Due to the three zones in the three-zone-model that can well match the "three vertical zones" after coal seam mining in Fig. 1 (elastic zone match the bending zone, plastic zone match the fractured zone and broken zone match the caved zone), the three-zone-model was used to further analyze the evolution of gas flow rates and gas pressure in the different vertical zones. The permeability of the plastic zone and elastic
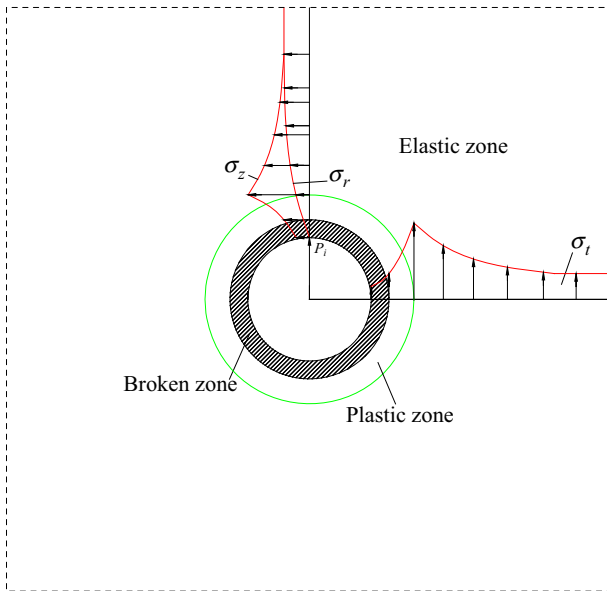
Fig. 10 Elastoplastic analysis model of drilling for surrounding rocks

zone can be updated according to Fig. 8. The broken zone in the three-zone-model was used to match the caved zone. While the gas pressure in caved zone changes little, this makes the permeability unchanged. Certainly, the change of gas pressure has an effect on the permeability of broken zone. However, due to the very high permeability of the broken coal samples, the gas pressure difference is difficult to exceed 0.5 MPa due to the limit of gas flowmeter range. In the measurable gas pressure range, the change of permeability is very small. Besides, the area of the broken zone is relatively small; its permeability has little effect on the average permeability change of the near-wellbore area. Considering the above factors, the permeability of broken zone is assumed to be unchanged. It is important to note that the permeability of the broken zone was changed in the mechanical calculation due to the stress changes (Zhang et al. 2017).

The cohesive softening model can calculate the area of the zone around the borehole (Huang et al. 2013). The softening formula for cohesive force in the plastic zone is as follows:

$$c = c_s + j_c(r - R) \tag{13}$$

where c_s is the residual cohesion along the edge of the borehole, j_c is the gradient of cohesion in the plastic zone, r is the distance from the plastic zone to the center of the drilling, and R is the drilling radius. j_c can be calculated using Eq. (14):

$$j_c = \frac{c_0 - c_s}{R_S - R} \tag{14}$$

where c_0 is the cohesive force of the elastic coal sample, and R_S is the actual radius of the plastic zone. To perform this simulation, the cohesive softening model was embedded in FLAC3D using the FISH language, and the plastic zone was calculated as shown in Fig. 11a.

After calculation of the mechanics, the gas pressure of the whole model was determined to be 3.7 MPa, and the negative drilling pressure was set at 0.05 MPa. The original permeability calculated according to the permeability update program (Fig. 8) is shown in Fig. 11b.
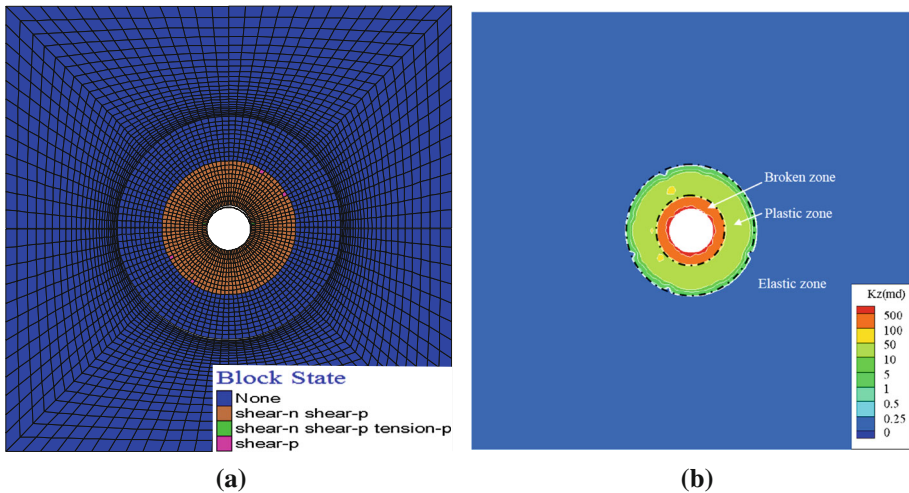
Fig. 11 Permeability and plastic distribution of drilling for surrounding rocks. **a** Plastic distribution, **b** permeability distribution

4.2 Simulation Results Analysis

The numerical simulation results fit the theoretical results well, indicating that the permeability of the coal seam around a drilling area experiences an obvious zoning phenomenon. Permeability is highest in the broken zone; it is lower in the plastic zone, but still much higher than in the elastic zone. The radius of each zone is very small, and drilling excavation has no obvious influence on permeability. However, pressure relief mining has an important influence on borehole stability and it is, therefore, necessary to reinforce boreholes during pressure relief mining. A great deal of research not detailed here has been conducted on the stability and reinforcement of boreholes (Chen et al. 2012; Whittles et al. 2007; Xue et al. 2015).

This simulation process accounted for the pressure relief effect of protective coal seam mining by reducing the vertical stress of the model from 22.5 to 6 MPa, while reducing the horizontal stress to 7.2 MPa. The increase in permeability in the elastic zone was obviously limited, as the permeability remained below 0.25 md, far lower than in the plastic zone. This indicates that increased coal seam permeability is limited only by reducing coal seam stress; as such, coal seam permeability can be greatly improved in the plastic zone. Based on the calculation results for permeability, this study made updates to the program and carried out a gas drainage simulation. Figures 12 and 13 show the gas pressure and permeability at different drainage stages.

The data in Fig. 12, which show gas pressure changes with drainage time, demonstrate that the borehole drainage area gradually enlarged with extraction. Because of the high permeability of the broken zone and plastic zone, gas pressure decreased significantly and sank below 0.5 MPa after 100 h. However, gas pressure in the elastic zone remained basically unchanged, mainly because the permeability of the elastic zone was so small. As gas pressure in the plastic zone decreased, the permeability of the plastic zone also rose, as shown in Fig. 13. Permeability remained basically unchanged in the elastic zone because gas pressure did not change. These results suggest that coal seams should be located in the fractured zone during pressure relief mining in order to improve the efficiency of coal seam gas drainage.
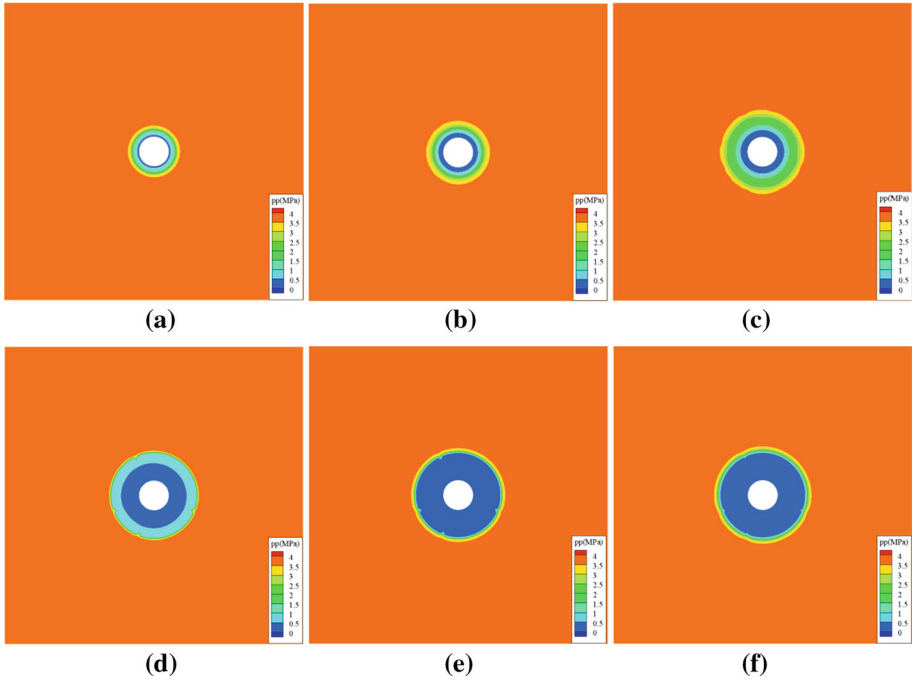
Fig. 12 Distribution of gas pressure in different extraction time. **a** 0.5 h, **b** 2 h, **c** 10 h, **d** 50 h, **e** 100 h, **f** 200 h
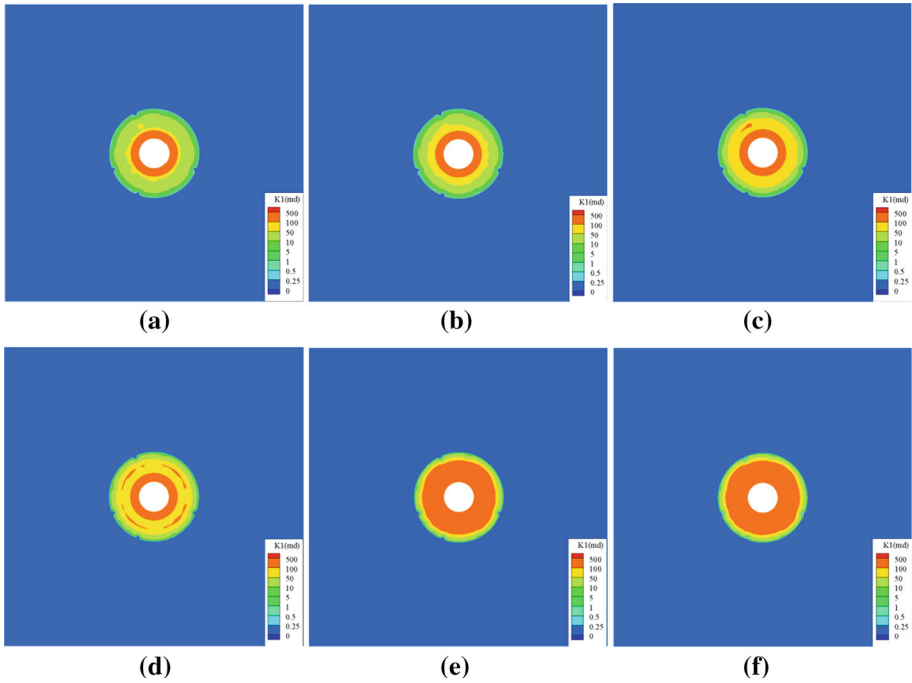

Fig. 13 Distribution of permeability in different extraction time. **a** 0.5 h, **b** 2 h, **c** 10 h, **d** 50 h, **e** 100 h, **f** 200 h

To address the evolution of gas pressure and permeability, monitoring points were arranged in the model as shown in Fig. 14a. Monitoring point 1 was located in the middle of the broken area, monitoring point 2 was located in the middle of the plastic zone, and monitoring points 3 through 5 were located in the elastic zone at increasing distances from the borehole. The results from each monitoring point are shown in Fig. 14b, c.

As extraction time increases, the gas pressure in the broken zone decreases rapidly; this may result in the phenomenon of gas outburst. The use of the variable permeability method (2#) simulates a situation in which gas pressure in the plastic zone decreases faster than in situations in which relative permeability is constant (U2#). This is more consistent with the actual gas pressure reduction in the plastic zone during the process of gas extraction. The evolution of the gas extraction rate and the average permeability of the model are shown in Fig. 15. The gas extraction rate rises sharply at first and then decreases gradually, consistent with the law of evolution for the ground gas drainage borehole extraction rate (Zhang et al. 2015). This finding demonstrates the reliability of this numerical simulation. The changes of average permeability of the model are similar to the plastic zone. As gas pressure decreases, the permeability of the plastic zone increases inconsistently in four stages: rapid increase, gradual smoothing, second slow increase, and ultimate stability. The main reasons for these changes are the sensitivity of the plastic zone to gas pressure and the decrease of gas pressure in the plastic zone. The experimental results displayed in Fig. 7 show that gas pressure sensitivity increases gradually with decreases in gas pressure; at the same time, the magnitude of the decrease in gas pressure decreases gradually during the gas extraction process. These findings indicate that the rapid increase stage in plastic zone permeability is caused by a large reduction in gas pressure. The second slow increase stage occurs because the decrease in gas pressure leads to increase stress sensitivity in relation to permeability. The gas pressure in the elastic zone decreases slightly because of the low permeability, but only in the monitoring area near the plastic zone (3#). Furthermore, the gas pressure in the elastic zone begins to decrease when the plastic zone's gas pressure falls below 0.1 MPa. Accompanied by decreasing gas pressure in the elastic zone, permeability at the monitoring points changes according to a "V" pattern, characterized by an initial decrease and subsequent increase. However, due to a slight decrease in gas pressure and relatively high external stress, permeability only changes slightly. These simulation results are basically consistent with the theoretical analysis, physical simulation, field test, and laboratory test results described in this paper and other papers (Chen et al. 2011; Coletta and Sicco 2012; Tao et al. 2012; Clarkson and Salmachi 2017; Salmachi and Karacan 2017).

5 Discussions

This paper described an experimental study carried out on the external stress-gas pressure–permeability relationship in elastic and shear failure coal samples. The permeability evolution of elastic and plastic fracture coal samples under different gas pressure and external stress conditions were well present. Building on this experiment, this paper proposed an external stress–gas pressure–permeability model for the plastic and elastic zones during pressure relief gas drainage. The external stress–gas pressure–permeability model is the fitting equation in this paper although it can well match the experiment results. Thus, for other geological settings, it needs to perform the laboratory measurement of permeability again. This will reduce the applicability of the fitting model. However, the most frequently used models such as P&M, C&B, S&D and others are also need to fit the experimental date to
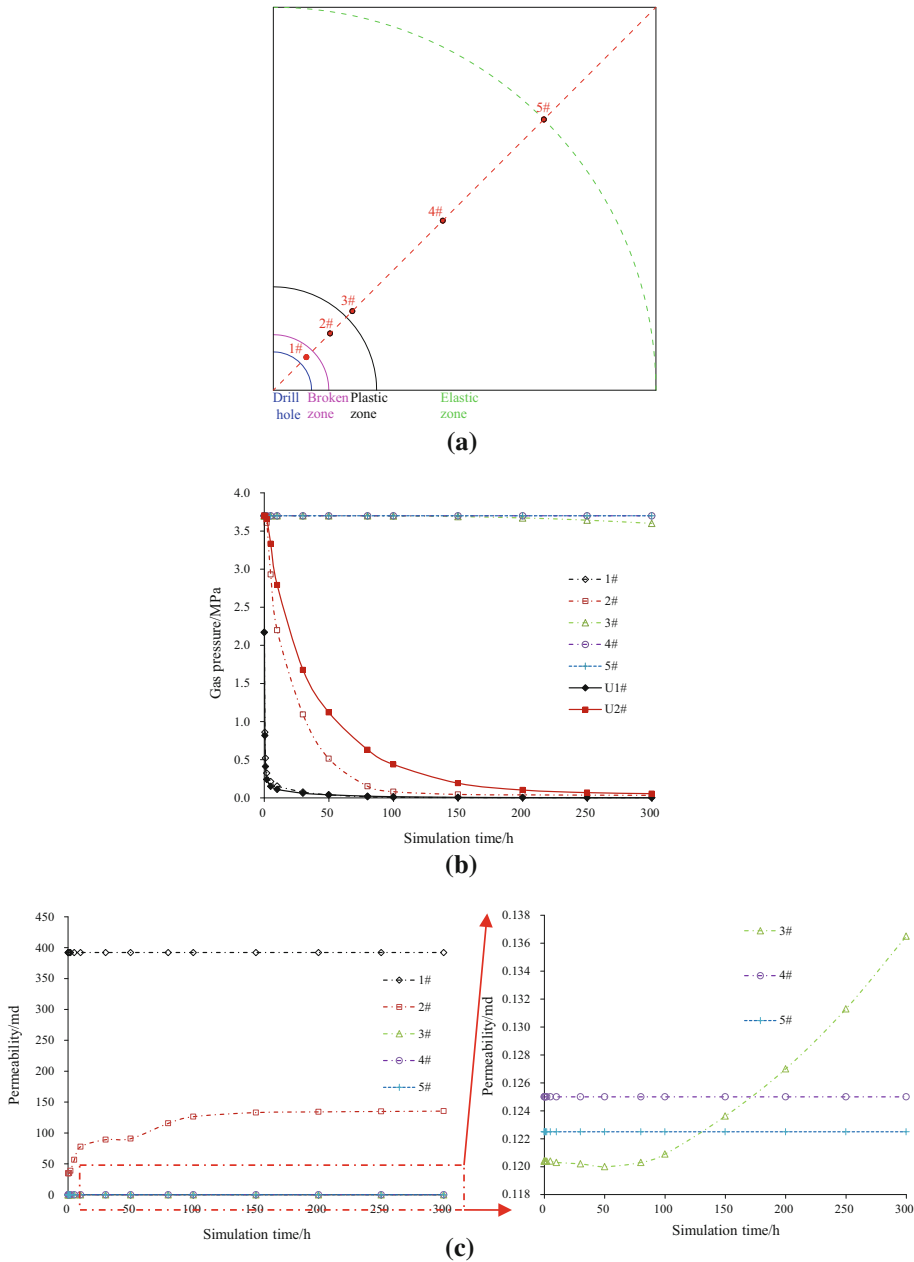
(a)

(b)

(c)

Fig. 14 Layout of monitoring points and its monitoring results. **a** Layout of monitoring points, **b** gas pressure, **c** permeability

quickly determinate the parameters and coefficients (cleat volume compressibility c_f, grain compressibility β, fraction f, and others). Besides, the above models need to obtain some other mechanical parameters such as modulus of pore volume K_p for C&B model and the
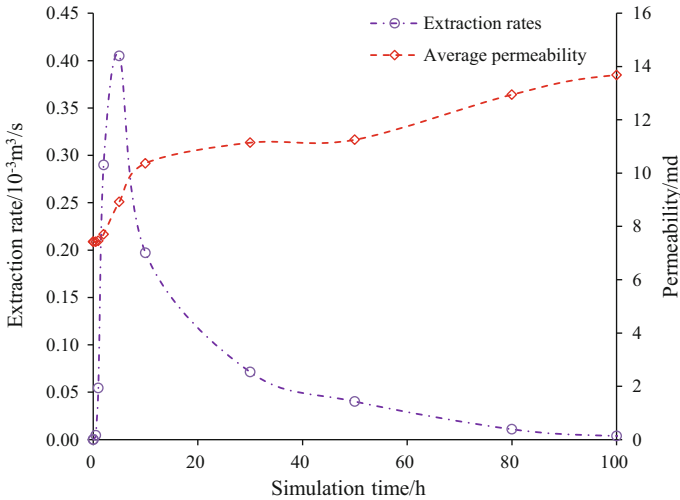
Fig. 15 Evolution of extraction rate and the average permeability of the model

constrained axial modulus *M* for P&M model. This is not conducive to the use of FISH language embedded in FLAC3D to study the permeability changes during pressure relief gas drainage and coal mining. Thus, though these fitting equations in this paper cannot be directly applied to other geological conditions, but the fitting equations of other geological conditions can be also obtained by the method in this paper. In addition, in the process of permeability test, under the action of external stress, gas pressure, both types of coal samples may have elastoplastic deformation, which will have a great impact on the established model. Thus, in the final permeability models expressed by Eqs. (11) and (12), the external stress and gas pressure were considering in both types of coal samples. For the elastic coal samples, the uniaxial compressive strength of the elastic coal sample in this paper is 15.98 MPa; it can be seen from Table 2. And in this paper, the axial stress was always equal to the confining stress, as shown in Fig. 4; it is hydrostatic state of stress. Thus, it may be little new fractures at this stress state and the coal samples are basically in the elastic state; the main deformation for the elastic coal samples was the elastic deformation. For the plastic fracture coal samples, the gas is mainly flow along this main fracture and the elastoplastic deformation has little influence in the total flow rates.

In addition to laboratory experiments, a numerical simulation of gas drainage according to the external stress–gas pressure–permeability model was conducted using the FISH language embedded in FLAC3D. The numerical results can well illustrate the changes of the permeability, gas pressure and the extraction rates. To simplify the calculation, the three-zone-model for gas extraction was used to analyze the evolution of gas flow rates and gas pressure so as to further study the flow characteristics in different vertical zones. Thus, the stress changes during the coal seam mining were not considered in the simulation. Besides, because the simulation in this paper examined protected coal seams, the only gas outlet in the coal seam was the drilling hole. In actual situations, pressure relief gas is released from the coal seam to the adjacent fracture zone; in that case, the gas pressure reduction rate is significantly greater than in the numerical simulation results. However, the numerical simulation results indicated that the simulation method in this paper can be used to simulate the evolution of permeability in different zones in Fig. 1. It provides a basis for simulating the gas drainage during the coal seam mining in the future.

6 Conclusions

Gas drainage in coal seam group pressure relief mining causes intense stress disturbance, while the external stress of a coal seam also changes with adjacent coal seam mining. Meanwhile, gas pressure decreases continuously in a coal seam during mining. Changes in gas pressure or external stress in turn cause changes in permeability. Therefore, it is necessary to consider these two factors during pressure relief gas drainage in order to provide guidance as to drilling location, drilling timing, and drilling pressure. Furthermore, severe stress disturbance can easily produce plastic yielding in a coal seam. Variations in coal seam permeability also differ between the elastic and plastic zones during the process of gas drainage. In this paper, an experimental study explored the relationship between external stress and gas pressure, and permeability in elastic and plastic fracture coal samples was carried out. And then conducts a numerical simulation of gas drainage according to the permeability model, using the FISH programming language embedded in the FLAC3D numerical simulation software. The main conclusions are as follows:

(1) Permeability in the elastic coal samples decreased first and then increased as gas pressure increased, consistent with the quadratic function curve under conditions of constant axial pressure and confining pressure. In contrast, permeability in the elastic coal sampled decreased with increasing gas pressure and did not appear to increase under constant effective stress. When gas pressure is less than the critical gas pressure, the Klinkenberg effect and matrix adsorption expansion play a major role in permeability changes. Decreases in effective stress lead to increases in pore space, and this process plays the leading role in permeability changes when the gas pressure exceeds the critical gas pressure.

(2) Unlike elastic coal samples, fractured coal samples experienced decreased permeability with increases in gas pressure, and permeability did not appear to increase at all within the range of gas pressure testing. The permeability of elastic coal samples significantly decreased with increasing gas pressure when gas pressure was less than 1 MPa. Subsequently, permeability decreased slowly as gas pressure continued to increase. The influence of the Klinkenberg effect and adsorption on permeability decreased with increasing gas pressure under the same effective stress or external stress conditions. Meanwhile, permeability and its sensitivity to gas pressure decreased with increases in effective stress or external stress. Based on these results, this paper provides a gas permeability model for elastic and plastic samples under different gas pressures and external stresses.

(3) Based on the theoretical formula of the laboratory tests, this paper established a calculation model for external stress, gas pressure, and permeability in the plastic and elastic zones during the process of gas drainage in coal seams. This model was embedded in FLAC3D using the FISH language to simulate gas pressure and permeability changes during pressure relief gas drainage. The simulation results show that permeability in the plastic zone increases in a nonlinear fashion as gas pressure decreases. These changes in permeability can be grouped into four stages: rapid increase, gradual smoothing, second slow increase, and ultimate stability. The simulation results strongly agree with the results measured in the field, indicating the reliability of the numerical simulation.

References

Cao, S.G., Guo, P., Li, Y., Bai, Y.J., Liu, Y.B., Xu, J.: Effect of gas pressure on gas seepage of outburst coal. J. China Coal Soc. **35**(4), 595–599 (2010)

Chen, J.G., Xu, P., Lai, Y.X., Du, Y.H.: Research on dynamic variation effect of coal reservoirs permeability. Rock Soil Mech. **32**(8), 2512–2516 (2011)

Chen, J., Wang, T., Zhou, Y., Zhu, Y., Wang, X.: Failure modes of the surface venthole casing during longwall coal extraction: a case study. Int. J. Coal Geol. **90–91**, 135–148 (2012)

Chen, Y., Liu, D., Yao, Y., Cai, Y., Chen, L.: Dynamic permeability change during coalbed methane production and its controlling factors. J. Nat. Gas Sci. Eng. **25**, 335–346 (2015)

Cheng, G., Ma, T., Tang, C., Liu, H., Wang, S.: A zoning model for coal mining—induced strata movement based on microseismic monitoring. Int. J. Rock Mech. Min. Sci. **94**, 123–138 (2017)

Clarkson, C.R., Salmachi, A.: Rate-transient analysis of an undersaturated cbm reservoir in australia: accounting for effective permeability changes above and below desorption pressure. J. Nat. Gas Sci. Eng. **40**, 51–60 (2017)

Coletta, M., Sicco, M.: Permeability increase in Bowen Basin coal as a result of matrix shrinkage during primary depletion. Int. J. Coal Geol. **96–97**(6), 109–119 (2012)

Cui, X., Bustin, R.M.: Volumetric strain associated with methane desorption and its impact on coalbed gas production from deep coal seams. Aapg Bull. **89**(9), 1181–1202 (2005)

Espinoza, D.N., Vandamme, M., Pereira, J.M., Dangla, P., Vidal-Gilbert, S.: Measurement and modeling of adsorptive-poromechanical properties of bituminous coal cores exposed to CO_2: adsorption, swelling strains, swelling stresses and impact on fracture permeability. Int. J. Coal Geol. **134**, 80–95 (2014)

Fathi, E., Tinni, A., Akkutlu, I.Y.: Correction to klinkenberg slip theory for gas flow in nano-capillaries. Int. J. Coal Geol. **103**(23), 51–59 (2012)

George, J.D.S., Barakat, M.A.: The change in effective stress associated with shrinkage from gas desorption in coal. Int. J. Coal Geol. **45**(2–3), 105–113 (2001)

Huang, L., Lu, Y.Y., Xia, B.W., Jia, Y.J., Huang, F.: Elastoplastic analysis of surrounding rock of drilling with strain softening model in deep soft rock. Rock Soil Mech. **34**, 179–186 (2013)

Jaeger, J.C., Cook, N.G.W., Zimmerman, R.W.: Fundamentals of Rock Mechanics. Blackwell Publishing, Malden (2007)

Klinkenberg, L.J.: The permeability of porous media to liquids and gases. Socar Proc. **2**(2), 200–213 (1941)

Li, B., Wei, J., Wang, K., Li, P., Wang, K.: A method of determining the permeability coefficient of coal seam based on the permeability of loaded coal. Int. J. Min. Sci. Technol. **24**(5), 637–641 (2014)

Liu, H.H., Rutqvist, J.: A new coal-permeability model: internal swelling stress and fracture-matrix interaction. Transp. Porous Media **82**(1), 157–171 (2010)

Lv, Y.: Test studies of gas flow in rock and coal surrounding a mined coal seam. Int. J. Min. Sci. Technol. **22**(4), 499–502 (2012)

Moghadam, A.A., Chalaturnyk, R.: Expansion of the Klinkenberg's slippage equation to low permeability porous media. Int. J. Coal Geol. **123**, 2–9 (2014)

Moghaddam, R.N., Jamiolahmady, M.: Fluid transport in shale gas reservoirs: simultaneous effects of stress and slippage on matrix permeability. Int. J. Coal Geol. **163**, 87–99 (2016)

Muljadi, B.P., Blunt, M.J., Raeini, A.Q., & Bijeljic, B.: The impact of porous media heterogeneity on non-darcy flow behaviour from pore-scale simulation. Adv. Water Res. **95**, 329–340 (2016)

Palchik, V.: Formation of fractured zones in overburden due to longwall mining. Environ. Geol. **44**(1), 28–38 (2003)

Palchik, V.: Experimental investigation of apertures of mining-induced horizontal fractures. Int. J. Rock Mech. Min. Sci. **47**(3), 502–508 (2010)

Palmer, I.: Permeability changes in coal: analytical modeling. Int. J. Coal Geol. **77**(1), 119–126 (2009)

Pan, Z., Connell, L.D., Camilleri, M.: Laboratory characterisation of coal reservoir permeability for primary and enhanced coalbed methane recovery. Int. J. Coal Geol. **82**(3), 252–261 (2010)

Salmachi, A., Karacan, C.Ö.: Cross-formational flow of water into coalbed methane reservoirs: controls on relative permeability curve shape and production profile. Environ. Earth Sci. **76**(5), 200 (2017)

Salmachi, A., Yarmohammadtooski, Z.: Production data analysis of coalbed methane wells to estimate the time required to reach to peak of gas production. Int. J. Coal Geol. **141–142**(1), 33–41 (2015)

Shi, J.Q., Durucan, S.: Exponential growth in San Juan Basin Fruitland coalbed permeability with reservoir drawdown: model match and new insights. SPE Reserv. Eval. Eng. **13**(6), 914–925 (2013)

Shi, J.Q., Durucan, S., Syahrial, E.: Reservoir depletion induced changes in coalbed permeability and implications for enhanced CBM recovery using CO_2 injection. Geol. Belg. **7**, 123–127 (2004)

Tao, S., Wang, Y., Tang, D., Xu, H., Lv, Y., He, W., Li, Y.: Dynamic variation effects of coal permeability during the coalbed methane development process in the Qinshui Basin, China. Int. J. Coal Geol. **93**, 16–22 (2012)

Wang, Y.F., Le, T.T.: A novel method for experimental evaluation on the sensitivity of gas flow velocity through rocks in gas layers. Nat. Gas Ind. **29**(10), 80–82 (2009)

Wang, H.L., Xu, W.Y., Chao, Z.M., Kong, Q.: Experimental study on slippage effects of gas flow in compact rock. Chin. J. Geotech. Eng. **38**(5), 777–785 (2016)

Wang, Z.P., Ran, Q.Q., Tong, M., Wang, C.M.: New forecasting method of fractured horizontal well productivity in volcanic gas reservoirs. Natural Gas Geosci. **25**(11), 1868–1874 (2014)

Whittles, D.N., Lowndes, I.S., Kingman, S.W., Yates, C., Jobling, S.: The stability of methane capture boreholes around a long wall coal panel. Int. J. Coal Geol. **71**(2–3), 313–328 (2007)

Xue, F., Zhang, N., Feng, X., Zheng, X., Kan, J.: Strengthening borehole configuration from the retaining roadway for greenhouse gas reduction: a case study. PLoS ONE **10**(1), e0115874 (2015)

Yao, X., Cheng, G., Shi, B.: Analysis on gas extraction drilling instability and control method of pore-forming in deep surrounding-rock with weak structure. J. China Coal Soc. **35**(12), 2073–2081(9) (2010)

Yarmohammadtooski, Z., Salmachi, A., White, A., Rajabi, M.: Fluid flow characteristics of bandanna coal formation: a case study from the fairview field, eastern australia. J. Geol. Soc. Aust. **64**(3), 319–333 (2017)

Yi, J., Akkutlu, I.Y., Karacan, C.O., & Clarkson, C.R. Gas sorption and transport in coals: A poroelastic medium approach. Int. J. Coal Geol. **77**(1), 137–144 (2009)

Yin, G., Jiang, C., Wang, J.G., Xu, J.: Geomechanical and flow properties of coal from loading axial stress and unloading confining pressure tests. Int. J. Rock Mech. Min. Sci. **76**, 155–161 (2015)

Yuan, M., Xu, J., Li, B., Cao, J., Zhang, M., Chen, Y.: Experimental study of permeability and deformation of anthracite during process of gaseous loading–unloading. Chin. J. Rock Mech. Eng. **33**(10), 2138–2146 (2014)

Zhang, C., Tu, S., Bai, Q., Yang, G., Zhang, L.: Evaluating pressure-relief mining performances based on surface gas venthole extraction data in longwall coal mines. J. Nat. Gas Sci. Eng. **24**, 431–440 (2015)

Zhang, C., Tu, S., Chen, M., Zhang, L.: Pressure-relief and methane production performance of pressure relief gas extraction technology in the longwall mining. J. Geophys. Eng. **14**(1), 77–89 (2017)

Zhou, Y., Li, Z., Yang, Y., Zhang, L., Si, L., Kong, B., Li, J.: Evolution of coal permeability with cleat deformation and variable Klinkenberg effect. Transp. Porous Media **115**(1), 153–167 (2016)

Affiliations

Cun Zhang[1,2,3] · **Lei Zhang**[4] · **Shihao Tu**[4] · **Dingyi Hao**[4] · **Teng Teng**[1,2,3]

✉ Cun Zhang
cumt_zc@163.com

Lei Zhang
leizhangcumt@163.com

[1] Beijing Key Laboratory for Precise Mining of Intergrown Energy and Resources, China University of Mining and Technology (Beijing), Beijing 100083, China

[2] School of Resource and Safety Engineering, China University of Mining and Technology (Beijing), Beijing 100083, China

[3] State Key Laboratory of Coal Resources and Safe Mining, China University of Mining and Technology, Beijing 100083, China

[4] School of Mines, Key Laboratory of Deep Coal Resource Ministry of Education of China, China University of Mining and Technology, Xuzhou 221116, Jiangsu, China